atoms

MDPI

Article

Assessment of Absorbed Dose from a Positron Beam in Biological Tissue and Its Potential for Radiotherapy

Andrezza O. Arêas and Maikel Y. Ballester *

Departamento de Física, Universidade Federal de Juiz de Fora, Juiz de Fora 36036-900, MG, Brazil; andrezza.areas@estudante.ufjf.br
* Correspondence: maikel.ballester@ufjf.br

Abstract

Fast-charged particles have been used in diagnosis and treatment since the 19th century. Positrons are widely used in medical imaging through positron emission tomography, but their therapeutic potential remains underexplored due to technology limitations associated with the lack of research on their effectiveness against cancer. One way to understand their behavior is by calculating absorbed dose distributions in tissue, which can be safely and realistically done using computational simulations such as the Monte Carlo Method. This study investigates the interaction of a positron beam with brain tissue and a tumor through simulations using the TOPAS software. Depth dose profiles and absolute absorbed dose values were obtained in the range of 6–24 MeV. Validation was performed using data from the water phantom with electron beams. The results showed that, at certain depths in brain tissue, the absorbed dose by positrons was higher than that of electrons under the same conditions, ranging from 57% to 463% more. These findings suggest that positrons may offer advantages over conventional electron therapy and contribute to the development of novel therapeutic approaches.

Keywords: positron therapy; brain tissue; tumor; TOPAS; Monte Carlo simulation

check for updates

Academic Editor: Grzegorz Piotr Karwasz

Received: 17 June 2025
Revised: 29 August 2025
Accepted: 2 September 2025
Published: 10 September 2025

Citation: Arêas, A.O.; Ballester, M.Y. Assessment of Absorbed Dose from a Positron Beam in Biological Tissue and Its Potential for Radiotherapy. *Atoms* **2025**, *13*, 78. https://doi.org/10.3390/atoms13090078

Copyright: © 2025 by the authors. Licensee MDPI, Basel, Switzerland. This article is an open access article distributed under the terms and conditions of the Creative Commons Attribution (CC BY) license (https://creativecommons.org/licenses/by/4.0/).

1. Introduction

The use of ionizing radiation for the treatment of diseases such as cancer dates back to the 1950s [1]. As technological development advanced, improvements in cancer treatment followed as well. Within ionizing radiation, a particular group of particles stands out, known as fast light-charged particles, characterized as "fast" because they approach the speed of light and "light" because they have a mass smaller than that of a proton [2]. These particles include electrons and positrons, and due to their ability to directly ionize the medium, they have many technological applications. One of these is in medicine, particularly in cancer diagnosis and treatment [3].

Electrons and positrons have been used since the 19th century in cancer treatment. Electrons are primarily employed in radiotherapy through the use of beams [1], and in brachytherapy, which involves the use of a source [4]. Both applications are well studied and firmly established, both theoretically and in clinical practice [5]. In turn, Positrons are used only in diagnostics, being applied in imaging exams such as positron emission tomography computed tomography (PET-CT), where their use involves radioactive sources [6,7]. Although positrons and electrons behave similarly when interacting with matter, with the exception of the annihilation phenomenon, positrons are not considered for cancer therapy, neither in beam form nor as a source [8].

The annihilation phenomenon occurs when a positron collides with an electron, resulting in the conversion of their mass into energy [2]. It can happen in two ways. The first is annihilation at rest, which typically occurs at the end of the positron's trajectory when it encounters an electron, as it reaches its thermalization energy—that is, when its energy is very low compared to its initial incident energy. Due to this characteristic, since the relative linear momentum between the positron and the electron is very low, they emit photons upon annihilation [9]. The other form of annihilation is called in-flight annihilation, in which a positron with an incident energy close to its initial value annihilates upon meeting an electron, also emitting photons [10]. The probability of this phenomenon occurring is rarer than annihilation at rest [11], as shown by the cross-section calculations obtained by Bethe [12].

Although there are currently several types of particle-based therapies, due to the difficulty and resistance in treatment [13], as well as the high mortality rate of the disease—about 10 million deaths and approximately 20 million new cases annually, according to the World Health Organization—developing new technologies or improving existing therapies remains necessary [14].

Some authors have investigated the effects of positrons and their effectiveness in cancer treatment [8,15,16]. Moadel reported, in both in vitro and in vivo studies conducted in 2003 and 2005, the potential for tumor and metastasis cure through positron-based treatment [15,16]. More recent studies by Hioki and collaborators demonstrated the effectiveness of positrons in causing single, and double, strand DNA breaks [8]. The underutilization of positrons is largely due to the lack of studies regarding their potential in cancer therapy and the safety concerns related to their use. For this reason, dosimetric calculations are essential to support the development of new technologies for their application.

One way to understand how positrons interact with matter is through dose calculation, which aims to observe and determine how the dose is distributed within the medium. This can be done using absolute values or, more commonly, through the calculation of the percentage depth dose (PDD) curve.

Monte Carlo method-based computer simulations are a safe and effective way to obtain reliable estimates of how particles interact within a given medium. This method allows for highly realistic simulations due to its stochastic and probabilistic nature, relying on cross-section calculations derived from experimental data and reference tables used within the scientific community. Currently, there are several simulation codes that offer robust and highly accurate results [17–19], providing reference values for theoretical model development and supporting experimental validation. Many works in the literature have employed this method and validated their results [19–22].

Motivated by this, the present work provides, for the first time, data on absolute dose distribution and PDD for a positron beam incident on a biological target, specifically, material representing brain tissue and a tumor, types of soft tissue, in an energy range between 6 and 24 MeV. The beam energies, ranging from 5 to 25 MeV, were selected to match the typical range for electron radiotherapy used in Brazil [23], where this research was conducted. The results are obtained through Monte Carlo simulation using the TOPAS software and are compared with simulations performed using electrons, highlighting the dose differences between the two particles.

2. Materials and Methods

In this study, the TOPAS software (Tool for Particle Simulation) (version 3.7.0) was chosen to perform the simulations, taking advantage of its advanced capabilities in radiation physics. TOPAS, in turn, uses version 10.06.p03 of Geant4 (Geometry and Tracking 4), a toolkit for simulating the passage of particles or radiation, which bases its simulations

on physical data tables and intrinsic interaction models. These tables and models provide crucial information about material properties and particle interactions with matter and are regularly updated and validated by the toolkit's developers and organizations responsible for supplying reliable data accepted by the scientific community. Examples include the International Commission on Radiation Units and Measurements (ICRU), the National Institute of Standards and Technology (NIST), and the International Commission on Radiological Protection (ICRP).

For such applications, the use of processors with a higher number of threads is necessary and recommended, as it significantly reduces the time required for each simulation. In this study, the following computer specifications were used:

Intel(R) Xeon(R) Silver 4310T CPU @ 2.30 GHz
Thread(s) per core: 1
Core(s) per socket: 10
Socket(s): 2
11th Gen Intel(R) Core(TM) i7-11700 @ 2.50 GHz
Thread(s) per core: 2
Core(s) per socket: 8
Socket(s): 1

In simulations, all generated secondary particles, such as electrons, photons, and ions, were tracked. The Geant4 default was used as the particle tracking cutoff, which applies a production cut of 1 mm. Secondary particles with a range below this value are not created; instead, their energy is accounted for as a local energy deposit. A total of 10^9 particles were simulated to minimize statistical uncertainties.

To calculate the absorbed dose distribution of positrons and electrons, it is necessary to define a well-structured geometry for the phantom. In this study, the phantom was modeled with a cubic geometry, with typical dimensions of $30 \times 30 \times 30$ cm^3, placed inside a parallelepiped filled with vacuum [24,25]. The cube was positioned so that the beam was directed toward the center of one of its faces. The phantom was divided into 100 bins, each with dimensions of $0.3 \times 30 \times 30$ cm^3, to record the amount of absorbed dose from positrons and electrons in each bin using the *DoseToMedium* scorer. The *DoseToMedium* scorer provides the absorbed dose in the medium after each simulation.

In the TOPAS model, monoenergetic electron and positron beams were emitted along the Z-direction. To evaluate the behavior of the particles, the distance between the beam and the phantom was set to 100 cm, which is a commonly recommended and used value in the literature, experiments, and simulation studies [24–26]. The irradiation field was set to 10×10 cm^2. The beam configurations used in the simulations are presented in Table 1:

Table 1. Beam parameters and scorer configuration used in the simulation.

Parameter	Configuration
BeamAngularDistribution	Flat
BeamAngularCutoffX and *Y*	2.8624 deg

The *BeamAngularDistribution* parameter defines the angular distribution of the particles in the beam. In this study, it was configured to distribute particles uniformly within a specific geometric area. This area is determined by the *BeamAngularCutoffX* parameter, which defines the irradiation field size.

2.1. Positrons and Electrons Beams Simulation on Water

For the validation of the methodology, the simulation settings were carefully defined to replicate the parameters used in the experiment, such as source-to-phantom distance, irradiation field size, and phantom material, thus ensuring comparability between the results obtained by both methods. These same parameters were also adjusted for comparison with simulation data available in the literature, including not only the experimental parameters but also the beam configurations.

The need to validate the methodology using electron beams in water arises from the lack of literature data on positron beams incident on any material within the energy range used in this work. In the absence of such data, validation must be performed using particles and media that are well-documented in the literature. This scarcity is partly due to the technological difficulty in producing positron beams at energies used in radiotherapy, and partly due to the limited number of studies exploring their potential in cancer treatment [8].

Thus, for comparison with experimental data from the literature (EL), three beams with different energies were used: 6, 9, and 12 MeV. For comparison with simulation data from the literature (SL), five beams with different energy values were used: 6, 9, 12, 20, and 24 MeV. The phantom composition used was the predefined material *G4_WATER*, which represents water. The choice of the energy range for both procedures was based on the typical energy levels used in radiotherapy [27], as well as the availability of data in the literature.

2.2. Positrons and Electrons Beams Simulation on Brain Tissue

After the validation of the methodology, positron beams with energies of 6, 9, 12, 20, and 24 MeV were simulated, and both the PDD and the absolute absorbed dose in each bin were obtained in order to generate data on the behavior of positrons in biological tissue. This is particularly important given the lack of literature data on positrons in this type of tissue and within this energy range. The phantom content used was brain tissue, representing the brain. The composition implemented for this simulation was not extracted directly from the program; it was taken from the reference document ICRU Report 44 [28]. Subsequently, electron beams with the same energies were simulated and the same quantities were calculated to enable a comparison of the behavior of both particles.

2.3. Positrons and Electrons Beams Simulation on Tumor

A simulation of a tumor within the brain was also performed, using two geometries. For the brain, the configuration of a cube with dimensions $30 \times 30 \times 30$ cm^3 was maintained, containing the same material described in the previous subsections. Inside the brain phantom, a cube with dimensions of $3 \times 3 \times 3$ cm^3 was inserted, located 2 cm from the front face of the brain and centered along the x and y axes. The material chosen for its composition was adipose tissue, which is predefined in the software as *ADIPOSE_TISSUE*. The distance between the brain phantom and the beam was kept constant, and the irradiation field used was 5×5 cm^2, which implies a configuration of the parameter *BeamAngularCutoffX* and *Y* = 1.4320 deg. A representation of the described geometry can be seen in Figure 1:

The tumor was divided into 200 bins to account for the dose distribution along the depth, and the total absorbed dose within the tumor volume was also obtained for both positrons and electrons, in order to compare the behavior of both particles.

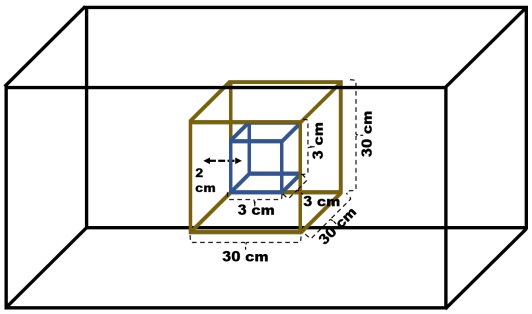


Figure 1. Geometric configuration used for simulating a tumor inside the brain.

For a complementary analysis, exploratory simulations of the positron and electron beam profiles were conducted to determine the particle's lateral spread. For such, the brain phantom was divided into 100 bins along the X and Z axes. An energy of 6 MeV was selected for this study due to its more significant scattering profile in contrast to the higher energies simulated. This choice is based on the principle that lower energy particles exhibit greater scattering [29,30], and the lateral profile curve was plotted at the depth of maximum dose d_{max} = 1.2 cm and at a depth near the end of the particle beam's range d = 3 cm.

3. Results

3.1. PDD Positrons and Electrons Beams Simulation on Water

In the simulation performed with the electron beam in water, the resulting curve is shown in Figure 2. When comparing the results of this work (SW) with the experimental PDD data obtained from the literature (EL), very similar behavior and well-fitted curves can be observed. It is noticeable that for the 6 MeV energy, the absorbed dose distribution reaches its maximum near the surface, while for the 9 and 12 MeV energies, the distribution is more gradual. These behaviors are expected and confirm that the methodology used is appropriate and valid for reproduction in other media, and can also be used to study the behavior of positrons.

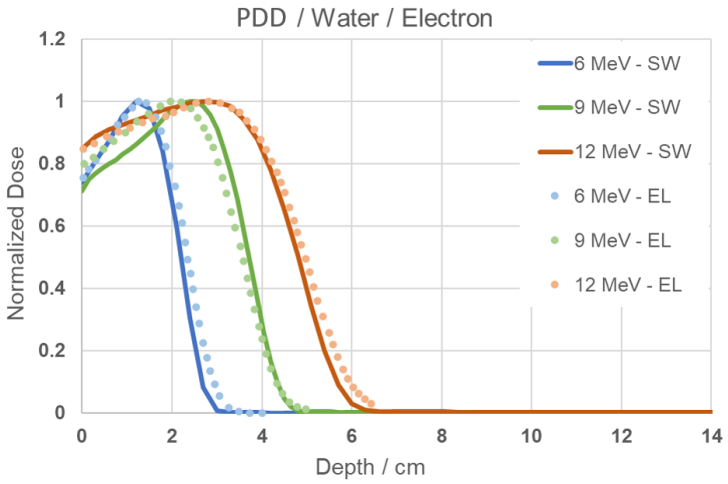


Figure 2. PDD Comparison graph of results from this study (SW) and experimental from literature data (EL) [24] for 6, 9, and 12 MeV energies.

In the simulation performed to compare the results obtained in this work (SW) with the electron simulation data available in the literature (SL) for electrons incident on water, it is possible to observe, through Figure 3, the similarity in behavior and excellent fit across all simulated energies.

The similarity in behavior with the results from Figure 2 for energies of 6, 9, and 12 MeV is also evident, with the maximum values of normalized dose remaining consistent, as well as the depths corresponding to the minimum PDD. For the energies of 20 and 24 MeV, the maximum PDD remains approximately at the initial 6 cm, indicating that the highest amount of absorbed dose is concentrated within this depth range, while the minimum PDD occurs at approximately 10 and 12 cm, respectively. When observing the behavior across all energies, it is noticeable that at higher energies, the maximum PDD is sustained over a broader range of depths, in addition to presenting less steep declines beyond this region.

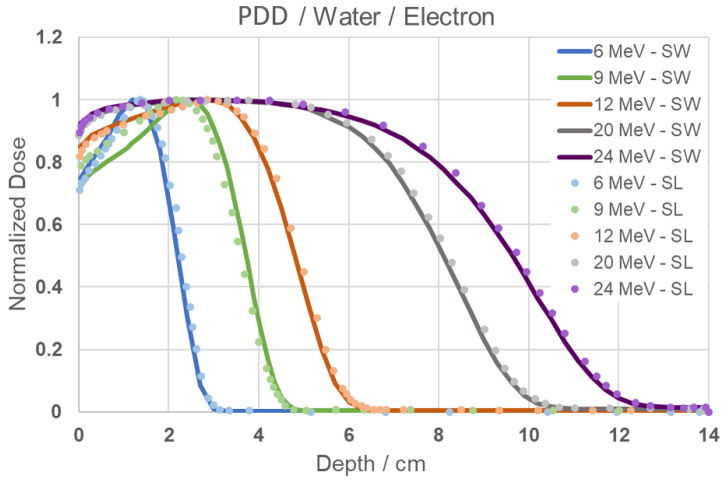


Figure 3. PDD Comparison graph of results from this study (SW) and simulation from literature data (SL) [24] for 6, 9, 12, 20 and 24 MeV energies.

Next, in order to compare the behavior between positrons and electrons in the same material, the simulation was carried out using a positron beam, for the same medium used previously, composed of water, and the results obtained can be seen in Figure 4. For the simulation of electrons in water at energies above 100 keV, the program utilized Møller cross-sections, and for positrons, Bhabha cross-sections [31]. For lower energies, the cross-sections developed for the PENELOPE package are used [32]. In this package, the Dirac equation is used for the elastic scattering of both particles, and their values differ due to the difference in the physical interaction [33]. Electrons are attracted by the nucleus and repelled by the orbital electrons, whereas positrons are repelled by the nucleus and attracted by the orbital electrons, thus leading to distinct values for this interaction. Inelastic scattering is described by the dielectric function and the Generalized Oscillator Strength (GOS) [32]. For electrons, this includes an exchange-effect term, while for positrons, this effect is absent, and other corrections are added. The annihilation interaction is based on the Dirac equation, as formulated by Heitler [34]. And for the Bremsstrahlung effect, data from Seltzer and Berger are used for both particles [35]; however, for positrons, a correction factor provided by NIST and ICRU is added to describe their interaction. Further details and the explicit form of the equations utilized by the program can be found in its documentation.

While the cross-sections for positron and electron interactions are different, they are essentially very similar when interacting with the same medium. From the PDD in Figure 4 the dose distribution of both particles in the same medium shows similar behavior for equal energies, and presents a shape that follows the same pattern as the results reported in the literature. The absorbed dose distribution is concentrated at the same depth for both particles with corresponding energies. It is also noticeable that for energies of 20 and 24 MeV, the PDD of both particles exhibits an extended region of maximum dose, rather than a single point, and in the case of positrons, it decreases slightly more in the 6 to 8 cm

interval compared to electrons, indicating that the percentage of absorbed dose in that region is reduced.

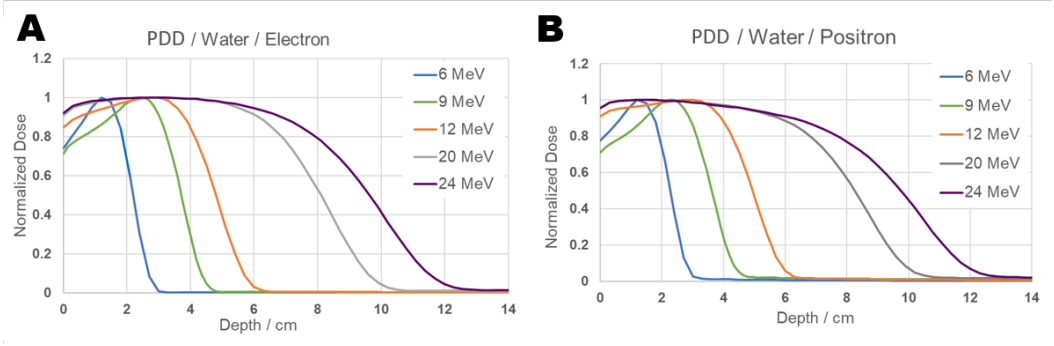


Figure 4. PDD Comparison graph of results from electron (Panel (**A**)) and positron (Panel (**B**)) beams inciding on water for 6, 9, 12, 20 and 24 MeV energies.

Individual dose curves for each energy are presented in Figure 5, where the differences in the positron and electron dose distributions can be visualized.

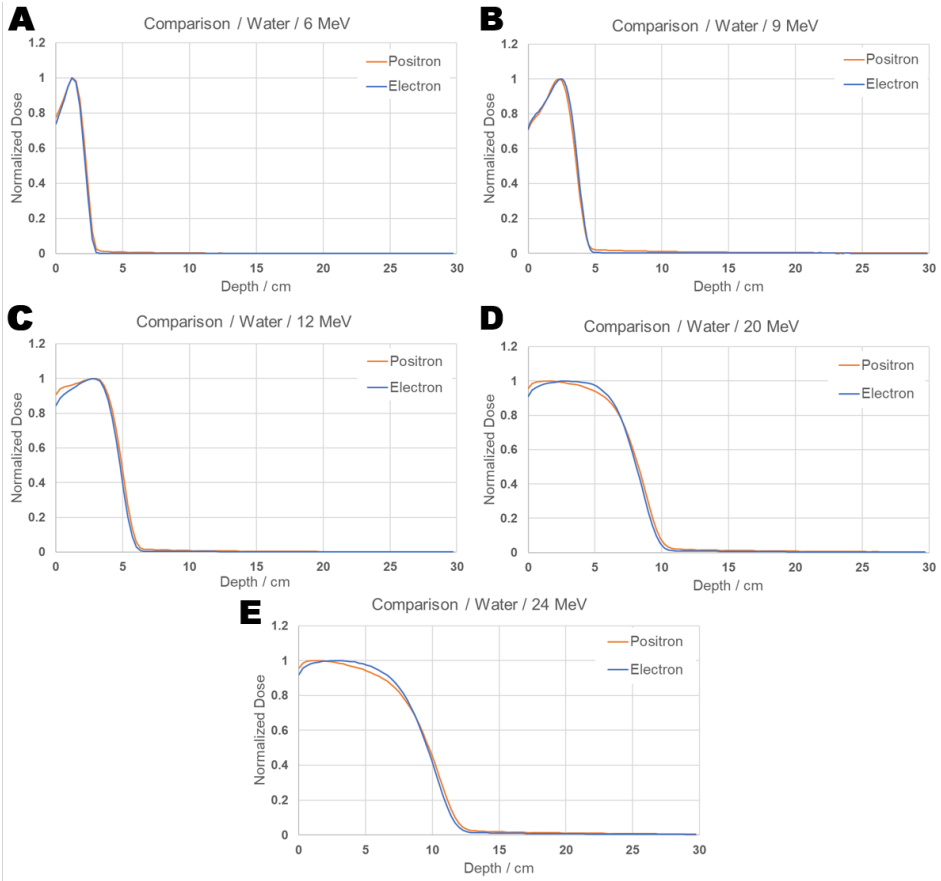


Figure 5. PDD comparison graph: Individual results from positron and electron beams inciding on water for energies 6 (**A**), 9 (**B**), 12 (**C**), 20 (**D**), and 24 (**E**) MeV.

3.2. PDD Positrons and Electrons Beams Simulation on Brain Tissue

The results obtained in this work for positron and electron beams incident on brain tissue can be seen in Figure 6:

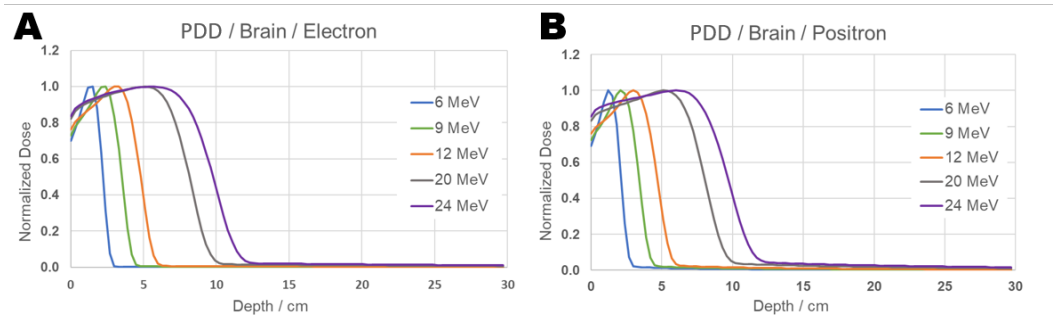


Figure 6. PDD Comparison graph of results from electron (Panel (**A**)) and positron (Panel (**B**)) beams incident on brain tissue for 6, 9, 12, 20, and 24 MeV energies.

As observed in the results and reports obtained in the literature for behavior in water, both particles incident on brain tissue show similar patterns, although similar, some small differences in the dose distribution along the depths between positrons and electrons, as can be seen at 20 MeV, indicating that a more detailed investigation may be warranted. For this purpose, the PDD comparison was performed at individual energies and is presented in Figure 7:

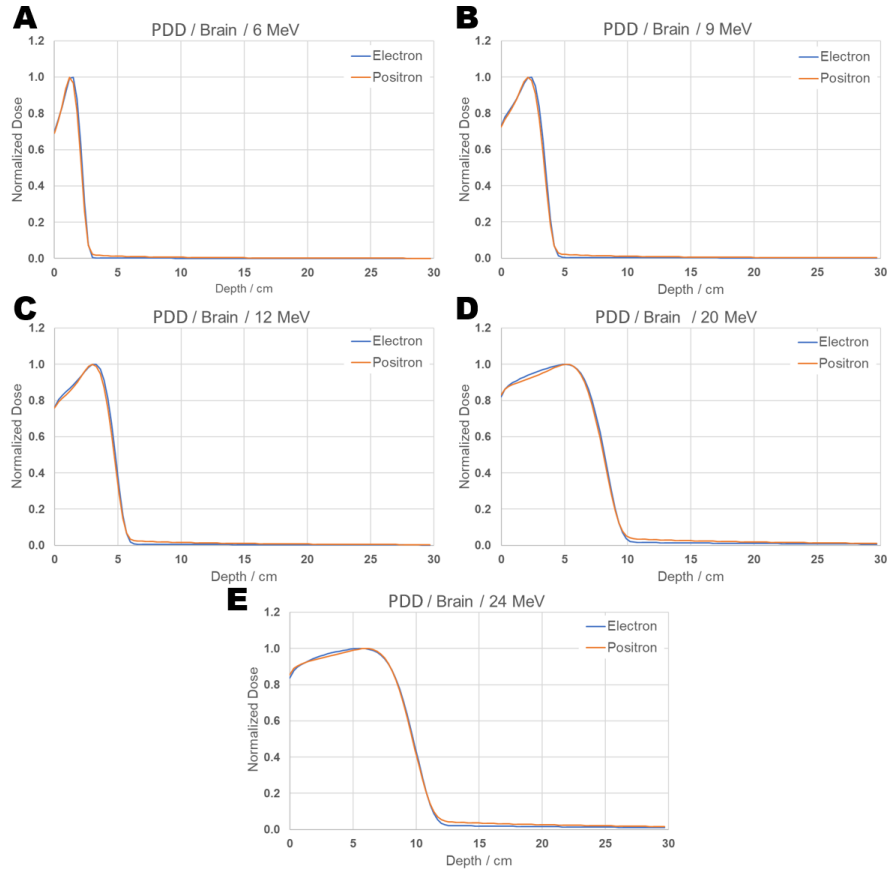


Figure 7. PDD comparison graph: Individual results from positron and electron beams incident on tissue brain for energies 6 (**A**), 9 (**B**), 12 (**C**), 20 (**D**), and 24 (**E**) MeV.

From the PDD evaluation, although the curves are largely similar, it is observed that, along the depth, the percentage of absorbed dose is sometimes lower at the beginning of the path and grows slightly less compared to electrons. For instance, at 6 MeV, the positron's maximum percentage dose occurs a few millimeters earlier than that of the electron. In the

cases of 20 and 24 MeV, the absorbed dose percentage in the first 5 cm is higher for electrons than for positrons.

Although such trends can be inferred from the graph, this analysis alone is not sufficient to determine whether the total absorbed dose is greater for one particle than the other, since the PDD represents a quantity normalized by the maximum absorbed dose value for each particle in the studied medium. Therefore, it was necessary to examine the absorbed dose in absolute values throughout each bin. Upon analyzing the results, a relevant difference in the absorbed dose between the two particles was observed, and this analysis is presented in Table 2:

Table 2. Average percentage difference of the dose absorbed by positrons compared to electrons as a function of depth.

Energy Range [MeV]	Depth Range [cm]	Mean Percentage Difference in Absorbed Dose
6 MeV		
	3.00–21.3	463%
	21.6–29.7	316%
9 MeV		
	4.80–14.1	285%
	14.4–28.8	183%
	29.1–29.7	161%
12 MeV		
	6.90–20.4	164%
	25.5–29.7	112%
20 MeV		
	12.6–20.1	99%
	20.4–29.7	71%
24 MeV		
	10.2–14.7	73%
	15.0–29.7	56%

From the calculation of the average percentage difference, it is possible to observe that, for the energy of 6 MeV, the absorbed dose of positrons in absolute values is approximately 460% higher than that of electrons in the range from 3 to 21.3 cm, considering point-by-point comparisons at the same depth, and about 300% higher between 21.6 and 29.7 cm. At 9 MeV, this difference ranges from approximately 285% to 160%, depending on the depth. For energies of 12, 20, and 24 MeV, the difference gradually decreases, yet remains from 164% to 56% higher than electrons, respectively, throughout the phantom. This demonstrates a significant difference between the two particles at specific depths within the same energy range, indicating a greater efficiency of positrons in depositing energy compared to electrons, depending on the material and its depth.

It is important to note that the results presented in this work have statistical uncertainties of less than 1%.

3.3. PDD Positrons and Electrons Beams Simulation on Tumor

The PPD obtained for positrons and electrons is presented in the Figure 8:

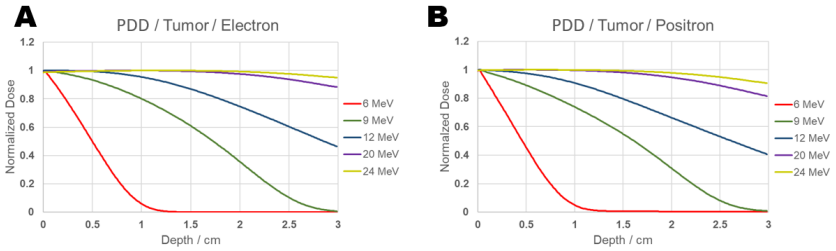


Figure 8. PDD comparison graph of results from electron (Panel (**A**)) and positron (Panel (**B**)) beams incident on tumor for energies 6, 9, 12, 20, and 24 MeV.

It can be observed from Figure 8 that, for an energy of 6 MeV, in the PDD curve, the maximum absorbed dose (100%) occurs at the beginning of the tumor at 0.015 cm, and 90% of the maximum dose is reached at a depth of approximately 0.1 cm for positrons, while for electrons the same percentage is found at 0.12 cm. For an energy of 9 MeV, 90% of the maximum dose occurs at 0.4 cm for positrons and at 0.645 cm for electrons. At 12 MeV, the same percentage is reached at 1.035 cm for positrons and at 1.32 cm for electrons. For 20 MeV, it is found at 2.4 cm for positrons and at 2.835 cm for electrons. At 24 MeV, 90% of the maximum dose reaches 3 cm, and for electrons, this same distance receives 95% of the maximum dose. The absolute values of absorbed dose representing the PDD between 90% and 100%—which correspond to the maximum dose values—are presented in Table 3 for positrons and in Table 4 for electrons.

Table 3. Absorbed dose with respective percentage and depth for positrons incident on the tumor.

Energy [MeV]	Absorbed Dose [Gy]	Percentage	Depth [cm]
6	3.39×10^{-2}	100%	0.015
6	3.08×10^{-2}	90%	0.100
9	3.97×10^{-2}	100%	0.015
9	3.58×10^{-2}	90%	0.465
12	3.72×10^{-2}	100%	0.015
12	3.36×10^{-2}	90%	1.035
20	3.57×10^{-2}	100%	0.450
20	3.22×10^{-2}	90%	2.415
24	3.57×10^{-2}	100%	0.615
24	3.23×10^{-2}	90.6%	2.985

Table 4. Absorbed dose with respective percentage and depth for electrons incident on the tumor.

Energy [MeV]	Absorbed Dose [Gy]	Percentage	Depth [cm]
6	3.72×10^{-2}	100%	0.015
6	3.37×10^{-2}	90%	0.120
9	4.14×10^{-2}	100%	0.015
9	3.73×10^{-2}	90%	0.645
12	3.91×10^{-2}	100%	0.090
12	3.52×10^{-2}	90%	1.335
20	3.76×10^{-2}	100%	0.870
20	3.39×10^{-2}	90%	2.835
24	3.75×10^{-2}	100%	1.260
24	3.57×10^{-2}	95.12%	2.985

Figure 9 shows the PDD curves for positrons and electrons at energies of 6, 9, 12, 20, and 24 MeV separately.

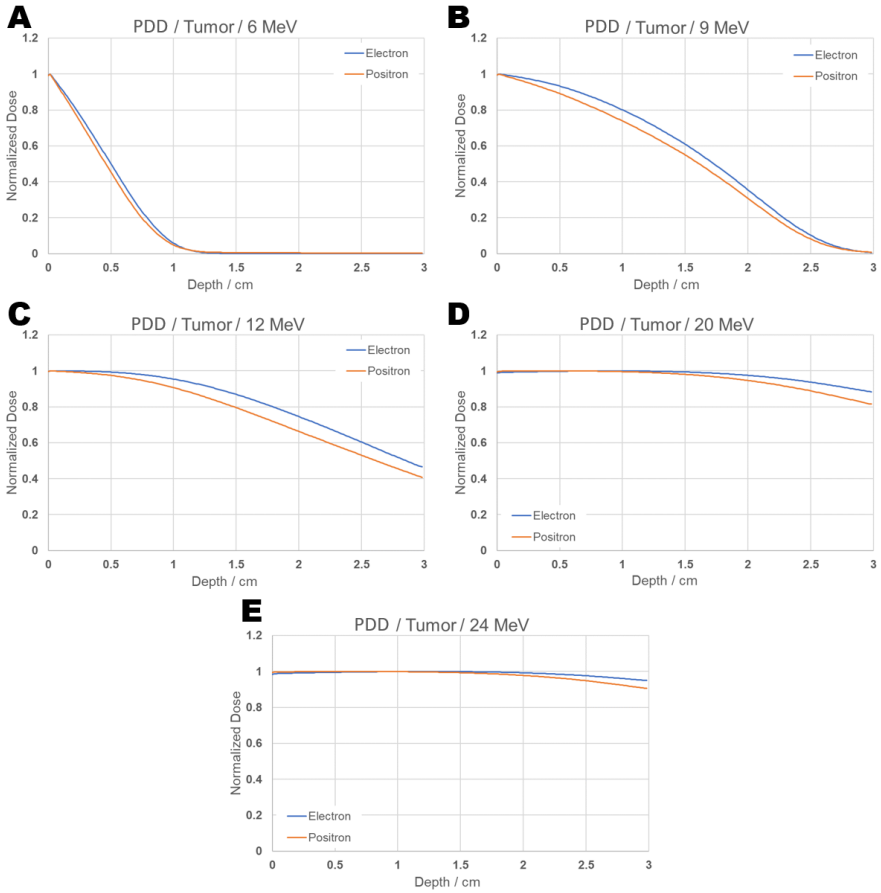


Figure 9. PDD comparison graph: Individual results from positron and electron beams incident on tumor for energies 6 (**A**), 9 (**B**), 12 (**C**), 20 (**D**), and 24 (**E**) MeV.

The results indicate that, according to the configurations selected in this study for the tumor, with the aim of avoiding exposure to healthy tissues, the recommended energies among those evaluated—both for positrons and electrons—would be 6 and 9 MeV. This is because, at 12 MeV, approximately 40% of the maximum dose reaches the end of the tumor depth, while at 20 and 24 MeV, about 90% of the maximum dose is still present at that same depth.

3.4. Absorbed Dose in the Tumor Volume

The total absorbed dose for the energies of 6, 9, 12, 20, and 24 MeV was calculated and is presented in Table 5:

Table 5. Total absorbed dose in the tumor volume.

Energy [MeV]	Total Dose Positron [Gy]	Total Absorbed Dose Electron [Gy]
6	5.67×10^{-3}	6.50×10^{-3}
9	2.02×10^{-2}	2.30×10^{-2}
12	2.88×10^{-2}	3.23×10^{-2}
20	3.42×10^{-2}	3.68×10^{-2}
24	3.50×10^{-2}	3.72×10^{-2}

Based on these values, it is possible to compare the total absorbed doses in the irradiated volume for both particles at different energies. It can be observed that, for the

calculated energies, the absorbed doses for positrons and electrons do not differ by orders of magnitude, and the differences between electrons and positrons for the energies of 6, 9, 12, 20, and 24 MeV are, respectively, 14.63%, 13.86%, 10.23%, 7.60%, and 6.28%.

For completeness, lateral profiles were also calculated at energy 6 MeV, and the results are displayed in the Figure 10. The analysis of the lateral profiles in Figure 10 reveals that the electron and positron beams exhibit equal pattern at maximum dose depth (1.2 cm), panel A, and at the depth corresponding to the beam's range (d = 3.0 cm), panel B. However, at the latter depth, a slightly larger scattering is observed for the positron beam compared to the electron beam. Still, the targeting quality for both types of particles in this energy range is very similar.

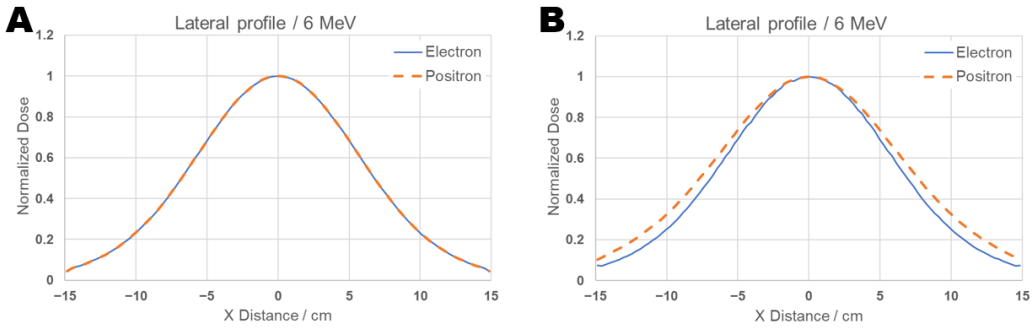


Figure 10. Comparative graph of the lateral beam profile for 6 MeV positrons and electrons on brain tissue with a tumor. The lateral profile curve was plotted at (**A**) the depth of maximum dose (d_{max} = 1.2 cm) and (**B**) the beam's range d = 3 cm.

4. Discussion

This study aimed to calculate the PDD of positrons in biological tissue targets, specifically brain tissue and a tumor region within the brain, through Monte Carlo simulation using TOPAS software. Due to the absence of data on positron beams in radiotherapy energy ranges for various tissues, the methodology used in this work was necessary to validate it. For that purpose, a water phantom with electron beams was used, because this is a well-documented medium and particle in the literature. The simulated data were validated against experimental results reported in the literature and also compared with published simulation results. The outcomes from this validation demonstrated that the data obtained in this study show good agreement with those reported in the literature, confirming that the methodology is appropriate and can be reproduced for positron studies.

The PDD of both particles was compared in the same medium to verify their behavior, and it was possible to observe similarities, such as the shape and dose distribution, which were concentrated at the same depths for both particles.

To assess the behavior of positrons incident on brain tissue, both the PDD and the absolute absorbed dose values along each bin were calculated. An electron beam was also simulated in the same medium and compared with positrons. This assessment made it possible to observe some similarities, such as the shape of the curve and the location of the PDD minimum occurring at the same depth for equivalent energies. However, some discrepancies were also observed in the normalized PDD. This led to a more detailed investigation of the dose profile, and for that, the absolute dose distribution along each bin was studied. When calculating the average percentage error of these values, it was observed that positrons have approximately 460% higher absorbed dose than electrons at certain depths, and, although this difference decreases with increasing simulated energy, it still remains approximately 56% higher than that of electrons.

For the simulation of a tumor located within the brain, the PDD, absolute absorbed dose values, and total absorbed dose within the tumor volume were obtained for both

positrons and electrons. From the PDD, it can be observed that for the tumor simulated in this study, the recommended beam treatment energies would be 6 and 9 MeV, since at higher energies, approximately 90% of the dose is still being delivered within 3 cm, the full length of the tumor, thus reaching brain tissue. When analyzing the total absorbed dose within the tumor volume, it was observed that electrons deliver a slightly higher absorbed dose than positrons, with values in the same order of magnitude and a difference not exceeding 15%. This indicates that although within the tumor volume electrons provide a slightly higher absorbed dose than positrons, when considering the absorbed dose in the brain, the value is significantly higher for electrons. This suggests that, depending on the tumor location, the use of positrons may be more advantageous.

The result showing that the absorbed dose of positrons is greater than that of electrons in brain tissue may be related to the total and partial cross sections of electrons and positrons [34]. While the total cross section describes the overall probability of a particle's interaction with a medium—being the sum of all partial cross sections—the partial cross sections represent specific interaction channels, such as elastic, inelastic, and annihilation processes [2,36]. To correlate these effects, it is necessary to address the differences between the cross sections used for positron-electron and electron-electron interactions. Their differences lie in how both particles interact with the nuclear Coulomb field and the electrons of the medium; while positrons are attracted by the medium's electrons and repelled by the nucleus, electrons exhibit the opposite behavior [37]. This characteristic implies a difference in the magnitude of the cross sections for these particles. There are also fundamental differences between the cross sections of both particles, which can be observed through well-known theoretical cross sections, such as Møller for electrons and Bhabha for positrons [37].

The Møller cross section's expression includes a term exclusive to electrons, also known as the exchange effect, which dictates that an electron can only transfer up to half of its energy to another electron [37]. For positrons, this effect does not occur due to the distinguishability of the particles; therefore, positrons can transfer from a small amount to all of their kinetic energy to an electron (provided the linear momentum is conserved). Another effect that differentiates positrons from electrons is the phenomenon of annihilation and positronium formation, which are introduced as correction functions in the cross-section expression. Such corrections are implemented by functions in the cross sections and depend only on the incident energy of these particles. These corrections are still studied today because they are known in a fragmented manner and need to be improved, a process in which a correlation with results from theoretical and experimental models is sought. The determination of cross sections for positrons and electrons is carried out by several authors, see for example Refs. [32,38–40], and their contributions are very important for observing and studying these differences, as well as for improving simulations. One consequence is the extra term from the exchange effect in the cross-section for electrons, which leads to a greater angular deviation in the particle's path, resulting in more dispersed trajectories [37]. Positrons, on the other hand, have a less scattered path because their cross-section is smaller due to the absence of this term. Having a less scattered trajectory can imply a greater absorbed dose within the medium. This is theoretically sound, as electrons, with their larger partial and consequently larger total cross sections, are subject to more trajectory deviations, which can occasionally cause them to exit the medium of interest. Furthermore, the annihilation term added to the positron's cross section can contribute to a higher absorbed dose for this particle, although more studies are needed to confirm these assertions.

Beyond the differences in the cross sections that govern the probability of interaction, a crucial point contributing to the observed dose differences is the distinction at the end

of the particle's trajectory. An electron, upon losing its kinetic energy, simply stops and is absorbed by the tissue, generating no more dose. The positron, in contrast, undergoes annihilation upon encountering an electron at the end of its path. This event is not just the end of the primary positron, but the beginning of a new energy deposition cascade. Annihilation converts the mass of the pair into gamma photons. These photons deposit their energy in the tissue through new interactions, ejecting secondary electrons. These new electrons, in turn, ionize the medium, creating an additional and localized source of absorbed dose. Therefore, annihilation can act as a dose amplification mechanism that is completely absent for electrons, being essential to explain the magnitude of the dosimetric advantage of positrons found in our study. This amplification in the number of events was observed in the simulations of this work by obtaining the StepCount scorer, which registered a much higher number of total interactions in the bins where the positron dose was maximal, potentially indicating the effect of the secondary particle cascade generated by annihilation.

The calculated contribution to the total doses deposited in the whole phantom from annihilation photons is rather small ($\leq 10^{-10}$ Gy). This property requires further investigation, and better strategies to control this radiation can be implemented, such as the insertion of magnetic fields to verify their effects on the dose distribution as well as on the particle behavior. Currently, there are technological limitations to produce positron beams of both high energy and sufficient flux for use in radiotherapy, which preclude their immediate clinical use. However, the results presented in this work show that positrons—from a beam or sources—have potential for their use in radiotherapy and not just for diagnosis in the fight against cancer. This is particularly interesting, as depending on the depth, positrons deliver a much higher absorbed dose than electrons. In turn, at the maximum depth of the dose, the lateral profiles calculated for positrons and electrons of 6 MeV show similar behavior. However, at the depth of the end of the beam range, positrons are somewhat more laterally scattered than electrons. This behavior can be attributed to the positron annihilation process and other secondary effects, like delta ray production, which lead to larger deviations of the beam. For both depths and particles, the deposited dose exhibits significant lateral scattering. This is an important issue, and eventually the use of magnetic fields could improve the targeting quality of both types of particles. Finally, by quantifying the therapeutic potential of positrons, our study explores the possibility of its application once technological advances enable accelerators to produce clinically viable positron beams, thereby spurring innovation in this field.

Author Contributions: A.O.A.: Conceptualization, Data curation, Formal analysis, Investigation, Methodology, Software, Validation, Visualization, Writing—original draft. M.Y.B.: Conceptualization, Funding acquisition, Methodology, Resources, Supervision, Writing—review & editing. All authors have read and agreed to the published version of the manuscript.

Funding: Financial support from Conselho Nacional de Desenvolvimento Científico e Tecnolgico' (CNPq) and FAPEMIG (Ref: BPD-00115-22) is acknowledged.

Data Availability Statement: Main data are reported in the article, while extra information can be supplied upon reasonable request.

Conflicts of Interest: The authors declare no conflicts of interest. The funders had no role in the design of the study; in the collection, analyses, or interpretation of data; in the writing of the manuscript; or in the decision to publish the results.

References

1. Keevil, S.F. Physics and medicine: A historical perspective. *Lancet* **2012**, *379*, 1517–1524. [CrossRef] [PubMed]
2. Yoshimura, E. Física das Radiações: Interação da radiação com a matéria. *Rev. Bras. FíSica MéDica* **2015** , *31* , 57–67.

3. Hogstrom, K.; Almond, P. Review of electron beam therapy physics. *Phys. Med. Biol.* **2006**, *51*, R455–R489. [CrossRef]
4. Chargari, C.; Deutsch, E.; Blanchard, P.; Gouy, S.; Martelli, H.; Guérin, F.; Dumas, I.; Bossi, A.; Morice, P.; Viswanathan, A.; et al. Brachytherapy: An overview for clinicians. *CA Cancer J. Clin.* **2019**, *69*, 386–401. [CrossRef]
5. Chang, D.; Lasley, F.; Das, I.; Mendonca, M.; Dynlacht, J. *Basic Radiotherapy Physics and Biology*; Springer International Publishing: Cham, Switzerland, 2014.
6. Nutt, R. The History of Positron Emission Tomography. *Mol. Imaging Biol.* **2002**, *4*, 11–26. [CrossRef] [PubMed]
7. Wagner, H.N. A brief history of positron emission tomography (PET). *Semin. Nucl. Med.* **1998**, *28*, 213–220 . [CrossRef]
8. Hioki, T.; Gholami, Y.; Mckelvey, K.; Aslani, A.; Marquis, H.; Eslick, E.; Willowson, K.; Bailey, D. Overlooked potential of positrons in cancer therapy. *Sci. Rep.* **2021**, *11*, 2475. [CrossRef]
9. Čížek, J.; Vlček, M.; Lukáč, F.; Melikhova, O.; Procházka, I.; Anwand, W.; Wagner, A.; Butterling, M.; Krause-Rehberg, R. Positron annihilation in flight: Experiment with slow and fast positrons. *J. Phys. Conf. Ser.* **2014**, *505*, 012043. [CrossRef]
10. Čížek, J.; Vlček, M.; Procházka, I. Investigation of positron annihilation-in-flight using a digital coincidence Doppler broadening spectrometer. *New J. Phys.* **2012**, *14*, 035005. [CrossRef]
11. Azuelos, G.; Kitching, J. The probability of positron annihilation-in-flight for allowed beta decay. *At. Data Nucl. Data Tables* **1976**, *17*, 103–105. [CrossRef]
12. Bethe, H.A. On the annihilation radiation of positrons. *Proc. R. Soc. Lond. Ser. A Math. Phys. Sci.* **1935**, *150*, 129–141. [CrossRef]
13. Mario; Migowski, A.; Ribeiro, C.; Franco, E.; Carvalho, F.; Claro, I.; Santos, M.; Mello, M.; Melo, M.; Rebelo, M.; et al. *ABC do câNcer: Abordagens báSicas para o Controle do câNcer [Basic Approaches to the Cancer Control—Revised 4th Edition and Updated]*; Instituto Nacional de Câncer José Alencar Gomes da Silva: Rio de Janeiro, Brazil, 2018.
14. International Agency for Research on Cancer, WHO. Cancer Today—Data Visualization Tools for Exploring the Global Cancer Burden, 2024. Available online: https://gco.iarc.who.int/today/en/dataviz/globe?mode=population&group_populations=0&types=1 (accessed on 20 February 2025.).
15. Moadel, R.M.; Nguyen, A.V.; Lin, E.Y.; Lu, P.; Mani, J.; Blaufox, M.D.; Pollard, J.W.; Dadachova, E. Positron emission tomography agent 2-deoxy-2-[18F]fluoro-D-glucose has a therapeutic potential in breast cancer. *Breast Cancer Res.* **2003**, *5*, R199–R205. [CrossRef]
16. Moadel, R.; Weldon, R.; Katz, E.; Lu, P.; Mani, J.; Stahl, M.; Blaufox, M.; Pestell, R.; Charron, M.; Dadachova, E. Positherapy: Targeted nuclear therapy of breast cancer with 18F-2-deoxy-2-fluoro-D-glucose. *Cancer Res.* **2005**, *65*, 698–702. [CrossRef]
17. Agostinelli, S.; Allison, J.; Amako, K.; Apostolakis, J.; Araujo, H.; Arce, P.; Asai, M.; Axen, D.; Banerjee, S.; Barrand, G.; et al. Geant4—A simulation toolkit. *Nucl. Instruments Methods Phys. Res. Sect. A Accel. Spectrometers Detect. Assoc. Equip.* **2003**, *506*, 250–303. [CrossRef]
18. Baró, J.; Sempau, J.; Fernández-Varea, J.; Salvat, F. PENELOPE: An algorithm for Monte Carlo simulation of the penetration and energy loss of electrons and positrons in matter. *Nucl. Instruments Methods Phys. Res. Sect. B Beam Interact. Mater. Atoms* **1995**, *100*, 31–46. [CrossRef]
19. Faddegon, B.; Ramos-Méndez, J.; Schuemann, J.; McNamara, A.; Shin, J.; Perl, J.; Paganetti, H. The TOPAS tool for particle simulation, a Monte Carlo simulation tool for physics, biology and clinical research. *Phys. Medica* **2020**, *72*, 114–121. [CrossRef] [PubMed]
20. Kaluarachchi, M.M.; Saleh, Z.H.; Schwer, M.L.; Klein, E.E. Validation of a Monte Carlo model for multi leaf collimator based electron delivery. *Med. Phys.* **2020**, *47*, 3586–3599. [CrossRef]
21. Rimchi, F.Z.; Moussa, A.; El Hamli, A.; Tayalati, Y. Monte Carlo Simulation of a Modified Elekta Precise Linear Accelerator Used for Flash Radiotherapy Using TOPAS (TOol for PArticle Simulation). In *Proceedings of the Advances in Smart Medical, IoT & Artificial Intelligence*; Serrhini, M., Ghoumid, K., Eds.; Springer: Cham, Switzerland, 2024; pp. 215–223.
22. Bedri, N.K.; Smetana, M.; Janousek, L. Impact of Metallic Implants on Dose Distribution in Radiotherapy with Electrons, Photons, Protons, and Very-High-Energy Beams. *Appl. Sci.* **2025**, *15*, 4536. [CrossRef]
23. Aguirre, E.; de Almeida, C.E.; David, M.G.; Venencia, D. Estudo da distribuição de dose de feixes clínicos de elétrons em meios heterogêneos. *Braz. J. Radiat. Sci.* **2020**, *8*, 1–18 . [CrossRef]
24. Contreras, E.H.A. Estudo das Distribuições de Dose em Meios não Homogêneos Usando Feixes Clínicos de Elétrons Através do Método de Monte Carlo. Master's Thesis , Universidade do Estado do Rio de Janeiro, Instituto de Biologia Roberto Alcântara Gomes, Rio de Janeiro, Brazil, 2018.
25. Neto, R.; Souza, F.; Fidelis, A.; Rocha, A.; Santana, L.; Rosa, L.; Cardoso, S. Simulações de experimentos didáticos em física médica com TOPAS MC. *Rev. Bras. Ensino Física* **2023**, *45*, 1–9 . [CrossRef]
26. Attix, F. *Introduction to Radiological Physics and Radiation Dosimetry*; A Wiley-Interscience Publication, Wiley: Hoboken, NJ, USA, 1986.
27. Cunha, J.S. Cálculo da Dose na Irradiação de Corpo Inteiro Utilizando Simuladores Antropomórficos Híbridos UF e o Código MCNPX. Master's Thesis, Universidade Federal de Sergipe, São Cristóvão, SE, Brazil, 2016.

28. International Commission on Radiation Units and Measurements. *Tissue Substitutes in Radiation Dosimetry and Measurement*; ICRU Report; International Commission on Radiation Units and Measurements: Bethesda, MD, USA, 1989; Volume 44 .
29. Khan, F.; Gibbons, J. *Khan's the Physics of Radiation Therapy*; Wolters Kluwer Health: Alphen aan den Rijn, The Netherlands, 2014.
30. Podgoršak, E.; Agency, I.A.E. *Radiation Oncology Physics: A Handbook for Teachers and Students*; International Atomic Energy Agency: Vienna, Austria, 2005; ISBN 9201073046.
31. Messel, H.; Crawford, D. *Electron–Photon Shower Distribution Function: Tables for Lead, Copper, and Air Absorbers*; Pergamon Press: Oxford, UK, 1970.
32. Salvat, F.; Fernández-Varea, J.; Sempau, J.; Penelope. A code system for Monte Carlo simulation of electron and photon transport. In *Workshop Proceeding* ; NEA Data Bank: Paris, France, 2007; pp. 4–7.
33. Perkins, S.; Cullen, D.; Seltzer, S. Tables and graphs of electron-interaction cross sections from 10 eV to 100 GeV derived from the LLNL Evaluated Electron Data Library (EEDL), Z = 1 to 100. *UCRL-50400* **1991**, *31*, 21–24. [CrossRef]
34. Heitler, W. *The Quantum Theory of Radiation*; International Series of Monographs on Physics; Clarendon Press: Oxford, UK, 1954.
35. Seltzer, S.M.; Berger, M.J. Bremsstrahlung energy spectra from electrons with kinetic energy 1 keV–10 GeV incident on screened nuclei and orbital electrons of neutral atoms with Z = 1–100. *At. Data Nucl. Data Tables* **1986**, *35*, 345–418. [CrossRef]
36. Davydov, A. *Quantum Mechanics*; Addison-Wesley series in advanced physics; Pergamon Press: Oxford, UK, 1965.
37. Rohrlich, F.; Carlson, B.C. Positron-Electron Differences in Energy Loss and Multiple Scattering. *Phys. Rev.* **1954**, *93*, 38–44. [CrossRef]
38. Mori, N.A.; Bray, I.; Fursa, D.V. Calculations of positron scattering and annihilation from H-like ions. *J. Phys. B At. Mol. Opt. Phys.* **2025**, *58*, 065201. [CrossRef]
39. Makochekanwa, C.; Sueoka, O.; Kimura, M. Similarities and differences between electron and positron scattering from molecules. *J. Phys. Conf. Ser.* **2007**, *80*, 012012. [CrossRef]
40. Zecca, A.; Chiari, L.; Trainotti, E.; Fursa, D.V.; Bray, I.; Sarkar, A.; Chattopadhyay, S.; Ratnavelu, K.; Brunger, M.J. Positron scattering from argon: Total cross sections and the scattering length. *J. Phys. B At. Mol. Opt. Phys.* **2012**, *45*, 015203. [CrossRef]

Disclaimer/Publisher's Note: The statements, opinions and data contained in all publications are solely those of the individual author(s) and contributor(s) and not of MDPI and/or the editor(s). MDPI and/or the editor(s) disclaim responsibility for any injury to people or property resulting from any ideas, methods, instructions or products referred to in the content.